Use of Polarimetric Measurements of the Sky over the Ocean for Spectral Optical Thickness Retrievals

KAZUHIKO MASUDA AND MASAYUKI SASAKI

Meteorological Research Institute, Tsukuba, Ibaraki, Japan

TSUTOMU TAKASHIMA

National Space Development Agency of Japan, Tokyo, Japan

HIROSHI ISHIDA

Maritime University of Kobe, Kobe, Hyogo, Japan

(Manuscript received 28 January 1998, in final form 28 August 1998)

ABSTRACT

To investigate the feasibility of retrieving spectral aerosol optical thickness from polarization measurements, the degree of polarization of the sky radiation was measured at a 90° angle from the solar direction in the principal plane with a multichannel polarimeter from ships on the Pacific Ocean and on the Inland Sea of Japan in 1997. The direct solar radiation was also measured simultaneously. Both measurements were made at wavelengths (λ) of 443, 490, 565, 670, 765, and 865 nm.

A lookup table of the degree of polarization with three parameters (the solar zenith angle, the aerosol optical thickness at $\lambda = 550$ nm, and the Ångström coefficient) was created from radiative transfer calculations. The aerosol model over the ocean is assumed to be composed of the externally mixed ''oceanic'' and ''water soluble'' components, whose size distributions are expressed by the lognormal functions. The size distribution parameters and refractive indices are adopted from the International Radiation Commission reports with a minor modification.

The effective aerosol optical thickness at $\lambda = 550$ nm and the Ångström coefficient were simultaneously retrieved from polarization measurements at $\lambda = 443$ and 865 nm by referring to the lookup table. The mean and standard deviation of the difference between the aerosol optical thickness retrieved from the polarization measurements and those determined from the direct solar radiation measurements were 0.00 and 0.02. The retrieved Ångström coefficients agreed well with those derived from the direct solar radiation measurements when the optical thickness exceeds 0.1, whereas the difference was about 0.5 when the aerosol optical thickness was only 0.05.

Sensitivities of the retrieval algorithm to the size distribution parameters and the refractive indices of aerosol models are also examined.

1. Introduction

Atmospheric aerosols play an important role in the earth radiation budget directly by scattering and absorbing solar and terrestrial radiation and indirectly by changing cloud properties. Accurate evaluation of the effects of the aerosols on the climate requires global information on aerosol properties such as optical thickness, size distribution, and refractive index.

Ground-based measurements of the atmospheric aerosols by optical instruments such as sun photometers, aureole meters, and polar nephelometers, are reported by many papers (DeLuisi et al. 1976a,b; Tanaka et al. 1983; Nakajima et al. 1986; Hoppel et al. 1990; Ahern et al. 1991; Takayama et al. 1991; Korotaev et al. 1993; Kaufman et al. 1994; Villevalde et al. 1994; Nakajima et al. 1996; and so on). Algorithms for retrieving the aerosol optical properties and their application to the atmospheric correction for new generation satellites such as the moderate-resolution imaging spectrometer are discussed by Kaufman et al. (1997), Tanré et al. (1996, 1997), Fraser et al. (1997), and Gordon (1997).

From an observational point of view, measuring the degree of polarization has an advantage in that absolute calibration of instruments may be eliminated because it is a relative value of the intensity of radiation. Measurements of the degree of polarization and analysis for retrieving aerosol optical properties have been reported

Corresponding author address: Dr. Kazuhiko Masuda, Dept. of Meteorological Satellite & Observ., Meteorological Research Institute, 1-1, Nagamine, Tsukuba, Ibaraki, Japan, 305-0052.
E-mail: masuda@mri-jma.go.jp

by Coulson (1980, 1983), based on the measurements from a mountain; Takayama et al. (1991) from a ship; Rao et al. (1973) and Deuzé et al. (1989) from balloons; Kawata and Yamazaki (1998) from an airplane; and Roger et al. (1994) from the U.S. Space Shuttle. Progressive theoretical studies have also been done by Mishchenko and Travis (1997), Leroy et al. (1997), Zhang and Gordon (1997), and Zhao et al. (1997).

Furthermore, the Polarization and Directionality of the Earth's Reflectances (POLDER) instrument (Deschamps et al. 1994), on board the Advanced Earth Observing Satellite (ADEOS), measured the degree and direction of polarization as well as the intensity of radiation from November 1996 to June 1997. The Earth Observing System-A/Earth Observing Scanning Polarimeter is also planned to be launched in the near future (WMO 1990).

To investigate the feasibility of using polarization measurements to retrieve aerosol optical properties over the ocean, we measured the degree of polarization of sky radiation as well as the direct solar radiation from ships on the Pacific Ocean and on the Inland Sea of Japan in August and September 1997. Sky radiation is basically influenced by the optical thickness, columnarly averaged size distribution, and refractive index of aerosols. To the best of our knowledge, however, practical algorithms to retrieve these parameters simultaneously from polarization measurements have not been developed. Tanré et al. (1996) pointed out that the spectral reflectance of a bimodal-lognormal distribution can be simulated well with spectral reflectance of a single lognormal distribution with an appropriate radius and width of distribution from their extensive numerical simulations for scattering angles of 102° and larger. Their results suggest that it is difficult to derive exact size distribution parameters uniquely from the measurements of scattered radiation that is not close to the solar direction. As suggested by Tanré et al. (1996), polarization may be more informative than the spectral radiance, but further investigations are necessary.

We limit the purpose of this paper to deriving the effective aerosol optical thickness and its spectral dependence from measurements of the degree of polarization by assuming a realistic aerosol size distribution model and the refractive index. The spectral dependence of aerosol optical thickness is simply expressed by the Ångström coefficient, which is the index α when the relationship between the wavelength (λ) (μm) and the aerosol optical thickness ($\tau_{a,\lambda}$) is expressed by $\tau_{a,\lambda} = \beta\lambda^{-\alpha}$ (Ångström 1964). A simple but stable inversion algorithm is proposed. The results are compared with those determined from the direct solar radiation measurements. Sensitivities of the inversion algorithm to the size distribution parameters and refractive indices of the aerosol model are also examined.

2. Atmosphere–ocean system model

The size distribution of atmospheric aerosols may be expressed by several functions such as the power-law function, the lognormal function, and the modified gamma function (Hansen and Travis 1974; d'Almeida et al. 1991). According to World Climate Programme (WCP) Radiation Commission reports (WCP-55 1983; WCP-112 1986), basic components of the maritime aerosol model are generally the ''oceanic'' model for the particles generated at the sea surface and the ''water soluble'' model for aerosols soluble in water and consisting of a mixture of sulfate, nitrate, and organic components. In this study, an externally mixed model of these aerosol components is assumed. This assumption is similar to those adopted by Tanré et al. (1996), Fraser et al. (1997), and Higurashi and Nakajima (1997) for retrieving the aerosol optical properties over the ocean from satellites. The size distribution for each aerosol model is expressed by the lognormal function

$$\frac{dn(r)}{d\ \ln r} = \frac{1}{\sqrt{2\pi}\ \ln\sigma} \exp\left[-\frac{(\ln r - \ln r_m)^2}{2\ \ln^2\sigma}\right], \quad (1)$$

where r_m is the median radius and $\ln\sigma$ is the standard deviation.

TABLE 1. Refractive index of aerosol components.

Wavelength (nm)	Oceanic	Water soluble
443	$1.38–8.01 \times 10^{-9}$	$1.53–5.00 \times 10^{-3}$
865	$1.37–1.20 \times 10^{-6}$	$1.52–1.21 \times 10^{-2}$

We first considered the WCP-112 model for the oceanic component and the WCP-55 model for the water soluble component. Table 1 shows the refractive indices of aerosol components at wavelengths (λ) of 443 and 865 nm (WCP-55 1983; WCP-112 1986). The r_m and σ values are given in Table 2 (oceanic, OC; water soluble, WS). These values of the refractive indices and size distribution parameters are basically the same as those compiled by Shettle and Fenn (1979) for the maritime aerosol model composed of continental and oceanic origin components at moderate relative humidities (70%–80% RH).

The scattering matrices are computed at wavelengths of 443, 490, 565, 670, 765, and 865 nm by the Mie scattering theory for radii ranging from 0.001 to 10.0 μm assuming the shape of aerosol particles to be spherical. The Ångström coefficients (α), which are calculated from the extinction coefficients, are also shown in Table 1. The Ångström coefficient for the oceanic model is much smaller than that for the water soluble model mainly because the oceanic model is composed of larger particles than the water soluble model. We define f_w as a ratio of the optical thickness of the water soluble component to the total aerosol optical thickness at $\lambda = 550$ nm ($\tau_{a,550}$). Then $\tau_{a,550}$ is expressed by

$$\tau_{a,550} = f_w\tau_{a,550} + (1 - f_w)\tau_{a,550} = \tau^{\mathrm{WS}}_{a,550} + \tau^{\mathrm{OC}}_{a,550}, \quad (2)$$

where $\tau^{\mathrm{WS}}_{a,550}$ is the optical thickness of the water soluble component at $\lambda = 550$ nm, and $\tau^{\mathrm{OC}}_{a,550}$ is that of the

TABLE 2. Size distribution parameters (r_m and σ) and Ångström coefficient (α) of aerosol components. Here OC denotes the oceanic model by WCP-112 (1986), WS the water soluble model by WCP-55 (1983). Subscript *snn* denotes that the original σ value is modified by multiplying the number of *nn*. Similarly, subscript *rnn* denotes that the original r_m value is modified by multiplying the number of *nn*.

Model	r_m (μm)	σ	α
OC	0.30	2.51	−0.10
OC_{s08}	0.30	2.01	−0.05
OC_{s09}	0.30	2.26	−0.09
OC_{s11}	0.30	2.76	−0.09
OC_{s12}	0.30	3.01	−0.09
OC_{r05}	0.15	2.51	0.05
OC_{r08}	0.24	2.51	−0.07
OC_{r12}	0.36	2.51	−0.11
OC_{r15}	0.45	2.51	−0.11
WS	0.0285	2.239	1.35
WS_{s08}	0.0285	1.791	2.57
WS_{s09}	0.0285	2.015	1.93
WS_{s11}	0.0285	2.463	0.93
WS_{s12}	0.0285	2.687	0.62
WS_{r05}	0.0143	2.239	1.96
WS_{r08}	0.0228	2.239	1.56
WS_{r12}	0.0342	2.239	1.18
WS_{r15}	0.0428	2.239	0.98

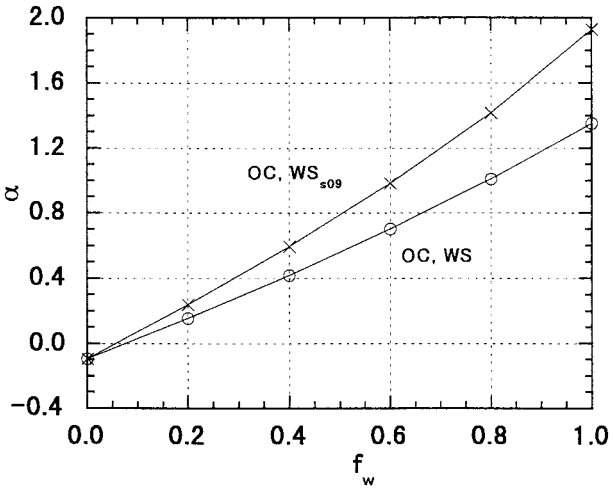

FIG. 1. Ångström coefficient (α) of the mixed aerosol model as a function of a ratio of the optical thickness of the water soluble component to the total aerosol optical thickness at $\lambda = 550$ nm (f_w). Circles denote the water soluble component by WCP-55, crosses by WCP-55, with the σ value decreased by 10%. In both cases, the oceanic component is adopted from WCP-112.

oceanic component. For the other wavelengths, the optical thickness of aerosol is given by

$$\tau_{a,\lambda} = \tau_{a,\lambda}^{\mathrm{WS}} + \tau_{a,\lambda}^{\mathrm{OC}}, \tag{3}$$

where

$$\tau_{a,\lambda}^{\mathrm{WS}} = \tau_{a,550}^{\mathrm{WS}} \beta_{\mathrm{ext},\lambda}^{\mathrm{WS}} / \beta_{\mathrm{ext},550}^{\mathrm{WS}}, \tag{4}$$

and

$$\tau_{a,\lambda}^{\mathrm{OC}} = \tau_{a,550}^{\mathrm{OC}} \beta_{\mathrm{ext},\lambda}^{\mathrm{OC}} / \beta_{\mathrm{ext},550}^{\mathrm{OC}}, \tag{5}$$

where β_{ext} are the extinction coefficients.

The Ångström coefficient for the mixed aerosol model obtained from $\tau_{a,\lambda}$ is shown in Fig. 1 (circles) as a function of f_w. The α values increase monotonically from −0.10 to 1.35 with increasing f_w. However, as shown in section 3, the Ångström coefficient derived from the direct solar radiation measurements ranges from −0.1 to 1.8. Therefore, this mixed aerosol model is not appropriate for retrieving the Ångström coefficient from our polarization measurements.

We therefore modified the size distribution parameters by changing the r_m value by 20% and 50% and the σ value by 10% and 20%. The Ångström coefficients of the modified aerosol components are also shown in Table 2. The α value for the water soluble component is clearly influenced by the change of these size distribution parameters, whereas that for the oceanic component is not changed so much. Considering these results, we adopted, as a reference model, the mixed aerosol model, which is composed of the original WCP-112 oceanic model and the WCP-55 water soluble model with σ decreased by 10%. Hereafter, we refer to these aerosol components as OC and WS_{s09} for simplicity. The Ångström coefficient for this mixed aerosol model is also shown in Fig. 1 (crosses). Now the α values range from −0.10 to 1.93. The radiative transfer calculation was done for eight $\tau_{a,550}$ values (0.0, 0.02, 0.04, 0.08, 0.16, 0.32, 0.64, and 1.28) and six f_w values (0.0, 0.2, 0.4, 0.6, 0.8, and 1.0).

The optical thicknesses of molecular scattering and absorbent constituents such as ozone were obtained from the Low-Resolution Transmission Model LOWTRAN7 for the midlatitude summer model (Kneizys et al. 1988). The depolarization factor of atmospheric molecules is 0.0295 according to Kneizys et al. (1980).

The ocean surface is simulated by multiple facets whose slopes vary according to the wind speed over the ocean (Cox and Munk 1954). Wind speed is assumed to be 5 m s^{-1}. The effect of white caps is not taken into account. The ocean is assumed to be homogeneous with an optical thickness of 10, and its bottom is assumed to absorb all radiation incident upon it. The ocean body is composed of pure water without hydrosols. As shown by Masuda and Takashima (1988), the downward radiation just above the ocean surface is little influenced by the oceanic condition.

The radiative transfer calculation was done by the doubling–adding method. A lookup table of the degree of polarization at a 90° angle from the solar direction in the principal plane was created with three parameters (the solar zenith angle; the aerosol optical thickness at $\lambda = 550$ nm; and the Ångström coefficient, which is determined from f_w). The computational method is the same as used by Masuda and Takashima (1988) where multiple scattering and polarization are taken into account. A plane-parallel and vertically inhomogeneous

atmosphere is simulated by four homogeneous sublayers (0–2, 2–5, 5–13, and 13–100 km).

3. Instruments and measurements

a. Multichannel polarimeter

Two similar multichannel polarimeters were used for measurements: one for the direct solar radiation, the other for the diffused sky radiation. The specification and calibration of the polarimeter are described in Masuda and Sasaki (1997). A brief description is given here. The multichannel polarimeter has six interference filters whose central wavelengths (half–transmission bandwidth) in nanometers are 443 (20), 490 (20), 565 (20), 670 (20), 765 (40), and 865 (40). These wavelength regions correspond to those of POLDER and the ocean color and temperature scanner sensors on board *ADEOS*. A Glan–Thompson prism is installed in front of the interference filters. The field of view is 2°. The detector is a silicon photodiode.

The basic sequence of polarization measurement of sky radiation is as follows. 1) The instrument on a tripod is manually pointed to a desired direction. 2) One of the interference filters is selected. 3) The prism is rotated to provide linearly polarized light to the interference filter. 4) The signal is successively transferred to a computer where the maximum and minimum signal values ($I_{\max}$ and $I_{\min}$) are stored. The degree of linear polarization (%) is obtained by $100 \times (I_{\max} - I_{\min})/(I_{\max} + I_{\min})$. This is equivalent to $100 \times |Q|/I$ for the principal plane, where I and Q are the first two components of the Stokes parameters.

Direct solar radiation, from which the aerosol optical thickness is derived, is also measured by the multichannel polarimeter. The operation is similar to the measurements of sky radiation except for what follows. First, the instrument is pointed in the solar direction. Second, the prism is not rotated. Third, the sequence of signal values is transferred to the computer where the maximum value is stored as the most probable value from which the optical thickness of aerosol is derived. Calibration constants were determined by the modified Langley plot at Mauna Loa Observatory in December 1996 and December 1997 (Masuda and Sasaki 1997).

b. Measurements of aerosols over the Pacific Ocean and the Inland Sea of Japan

The sky radiation and the direct solar radiation were measured over the Pacific Ocean from Kobe, Japan, to Honolulu, Hawaii, by the training ship (*Seiun-maru*) of the Institute for Sea-Training, Ministry of Transport of Japan, in August 1997. Similar measurements were made over the Inland Sea of Japan by the training ship (*Fukae-maru*) of the Maritime University of Kobe in September 1997. We refer to these cruises as the PO and the IS cruises, respectively. Measurements were made on six days when no clouds were observed between these directions and the ship motion is not so large (about ±3°).

The degree of polarization (p_{90}) was measured at a 90° angle from the solar direction in the principal plane, where the degree of polarization is generally maximum. This enables us to get stable values despite ship motions. Radiative transfer calculations showed that the deviation from the maximum value caused by the ship motion of ±3° was less than 1.5% in polarization units in the worst case at $\lambda = 443$ nm and 865 nm for the OC and WS_{s09} aerosol models for $\tau_{a,550} = 0.04$, 0.16, and 0.64. The accuracy of polarization measurements by the multichannel polarimeter is estimated to be about 1% in polarization units from the ground-based measurements (Masuda and Sasaki 1997). During the cruises, preliminary measurements of sky radiation at 2-min intervals showed that the reproducibility of the degree of polarization was about 1% under stable atmospheric conditions. Therefore, we estimate the accuracy of the measurements of degree of polarization to be generally better than 2% in polarization units including the effect of ship motion.

In the derivation of aerosol optical thickness from the direct solar radiation measurements, the error in calibration constant (c_λ) influences $\tau_{a,\lambda}$ as follows:

$$\Delta\tau_{a,\lambda} = \mu_0(\Delta c_\lambda/c_\lambda), \tag{6}$$

where μ_0 is the cosine of the solar zenith angle. For example, the 1% error of c_λ corresponds to an error of 0.005 in $\tau_{a,\lambda}$ for $\mu_0 = 0.5$ (solar zenith angle is 60°). The error in c_λ may be caused by the degradation of the interference filters. The c_λ values of the multichannel polarimeter changed by 0.7% to 2.7% depending on the wavelengths between two Langley plot calibrations at Mauna Loa Observatory in December 1996 and December 1997. We linearly interpolated the calibration constants for the periods of the PO and IS cruises. However, some uncertainties may exist. Even if c_λ remains constant, the solar radiation measurements are influenced by electrical noise, ship motions, and so on. During the cruises, preliminary measurements of the direct solar radiation at 2-min intervals were done under stable atmospheric conditions. The reproducibility of the derived optical thickness was better than 0.01. Furthermore, we estimated the effect of the sun's aureole contribution to the aerosol optical thickness according to Shiobara and Asano (1994) for the OC and WS_{s09} components. For the OC model, it was 0.002 and 0.01 for $\tau_{a,550} = 0.04$ and 0.2 at $\lambda = 443$ nm, and 0.0007 and 0.004 for $\tau_{a,550} = 0.04$ and 0.2 at $\lambda = 865$ nm, whereas it was less than 0.0002 for the WS_{s09} model. Thus, we estimate the accuracy of the measurements of the aerosol optical thickness determined from the direct solar radiation to be, in general, better than 0.02.

Table 3 shows the central ship position for each day. During the PO (IS) cruise, 61 (28) measurements of p_{90} and 26 (13) measurements of the direct solar radiation

TABLE 3. Location of the ships.

Date	Region	Latitude	Longitude
4 Aug 1997	Pacific Ocean	35.1°N	159.8°E
6 Aug 1997	Pacific Ocean	33.8°N	173.1°E
9 Aug 1997	Pacific Ocean	28.0°N	169.7°W
11 Aug 1997	Pacific Ocean	21.2°N	159.8°W
28 Sep 1997	Inland Sea of Japan	34.5°N	134.5°E
29 Sep 1997	Inland Sea of Japan	34.5°N	134.7°E

were made. The p_{90} values were averaged when two or more measurements were made within 5 min and differences of p_{90} values were less than 3% for every channel. The aerosol optical thickness determined from the direct solar radiation [$\tau_{a,\lambda}$(dir)] at the time of polarization measurement was interpolated from the adjacent values for each wavelength. The Ångström coefficient [α(dir)] was then calculated from $\tau_{a,\lambda}$(dir). The aerosol optical thickness at $\lambda = 550$ nm [$\tau_{a,550}$(dir)] was interpolated from $\tau_{a,490}$(dir) and $\tau_{a,565}$(dir). Thus, 19 (12) measurement datasets were created for the PO (IS) cruise. The solar zenith angles were from 27.6° to 57.9° (PO) and from 38.8° to 57.2° (IS).

Figure 2a shows the aerosol optical thickness at $\lambda = 550$ nm [$\tau_{a,550}$(dir), circles], and the Ångström coefficient [α(dir), crosses] derived from the measurements of the direct solar radiation. On 4 August, $\tau_{a,550}$(dir) was about 0.16 and α(dir) was stable at around 1.0. On the other days in the PO cruise, $\tau_{a,550}$(dir) was very low. The corresponding α(dir) values range from -0.1 to 0.5. Figure 2b shows the correlation coefficients between $\ln\tau_{a,\lambda}$(dir) and $\ln\lambda$. This correlation coefficient may be a measure of the smoothness of the optical thickness and wavelength relationship. The correlation coefficients were also calculated associated with the calculation of the Ångström coefficient by the Mie scattering theory for various aerosol models (section 2) showing the absolute values larger than 0.95. Therefore, the Ångström coefficient for small $\tau_{a,550}$(dir) values in Fig. 2a may not be reliable. However, the differences between $\tau_{a,\lambda}$(dir) and those approximated by the Ångström's equation $\beta\lambda^{-\alpha}$ were less than 0.005 for all measurements. These results show that the relative errors in $\tau_{a,\lambda}$(dir) become large for small aerosol optical thickness, which may result in unreliable Ångström coefficients.

Figure 2c shows the p_{90} values for $\lambda = 443$ nm (circles), 670 nm (crosses), and 865 nm (dots). It is seen that p_{90} values generally decrease with increasing the aerosol optical thickness. Furthermore, the wavelength dependence of the p_{90} values seems to be related to the optical characteristics of aerosols. For example, p_{90} at $\lambda = 865$ nm (dots) had similar values on 11 August and on 29 September, but the p_{90} values at $\lambda = 443$ and 670 nm (circles and crosses) are very different between these days.

4. Results

a. Theoretical background

Figure 3 shows the degree of polarization at a 90° angle from the solar direction in the principal plane (p_{90}) obtained by the radiative transfer calculations for the solar zenith angle of 45.8° where the aerosol optical thickness at $\lambda = 550$ nm ($\tau_{a,550}$) changes from 0.0 (no aerosols) to 1.28. Two extreme cases are shown for $f_w = 0$ (purely oceanic model, OC) and $f_w = 1$ (purely water soluble model, WS_{s09}). The p_{90} value should be 100% if the radiative transfer calculation were done for the molecule model considering only a single scattering with zero depolarization factor. However, it deviates from 100% due to the effects of the depolarization factor (assumed to be 0.0295) and multiple scatterings. The p_{90} value further decreases with increasing aerosol optical thickness. The decrease of p_{90} from the molecule model depends both on the wavelength and on the aerosol model. The effect of the difference of aerosol models appears more clearly in the longer wavelength regions due to the smaller molecular optical thickness (0.016 at $\lambda = 865$ nm but 0.237 at $\lambda = 443$nm). For the water soluble model (Fig. 3a), the decrease of p_{90} from the molecule model is generally larger at the shorter wavelengths than at the longer ones in spite of the greater molecule optical thickness. This is partly because the water soluble model has a large optical thickness at the shorter wavelength due to a large Ångström coefficient (1.93) and partly because the degree of polarization of single scattering at the 90° scattering angle is much smaller at short wavelength (33.5% at $\lambda = 443$ nm) than that at long wavelength (63.5% at $\lambda = 865$ nm). In contrast, the optical thickness of the oceanic model depends less on the wavelength because of a small Ångström coefficient (-0.10). Furthermore, the degree of polarization of single scattering is not very different between these wavelengths (-10.4% at $\lambda = 443$ nm and -8.3% at $\lambda = 865$ nm). Consequently, the effect of aerosol is more at the longer wavelength region due to small molecule optical thickness (Fig. 3b). Thus the wavelength dependence of p_{90} is a good indicator of the aerosol model and optical thickness.

The relationship of the p_{90} between two wavelengths obtained from the radiative transfer calculations is shown in Fig. 4 as a function of $\tau_{a,550}$ and α. Three wavelength pairs are shown out of 15 combinations of six wavelengths. Note that the uppermost (lowermost) curves labeled by 1.93 (-0.10) correspond to the purely water soluble (oceanic) model (Fig. 3). Only the results for the solar zenith angle of 45.8° are shown. However, the p_{90} value is not significantly influenced by the solar zenith angle. In our calculations, the difference of p_{90} values was less than 2% in polarization units for the solar zenith angles between 22.5° and 60°. The measurements are also plotted in the figures where circles denote measurements in the PO cruise, and crosses denote the IS cruise. This figure suggests that it is possible

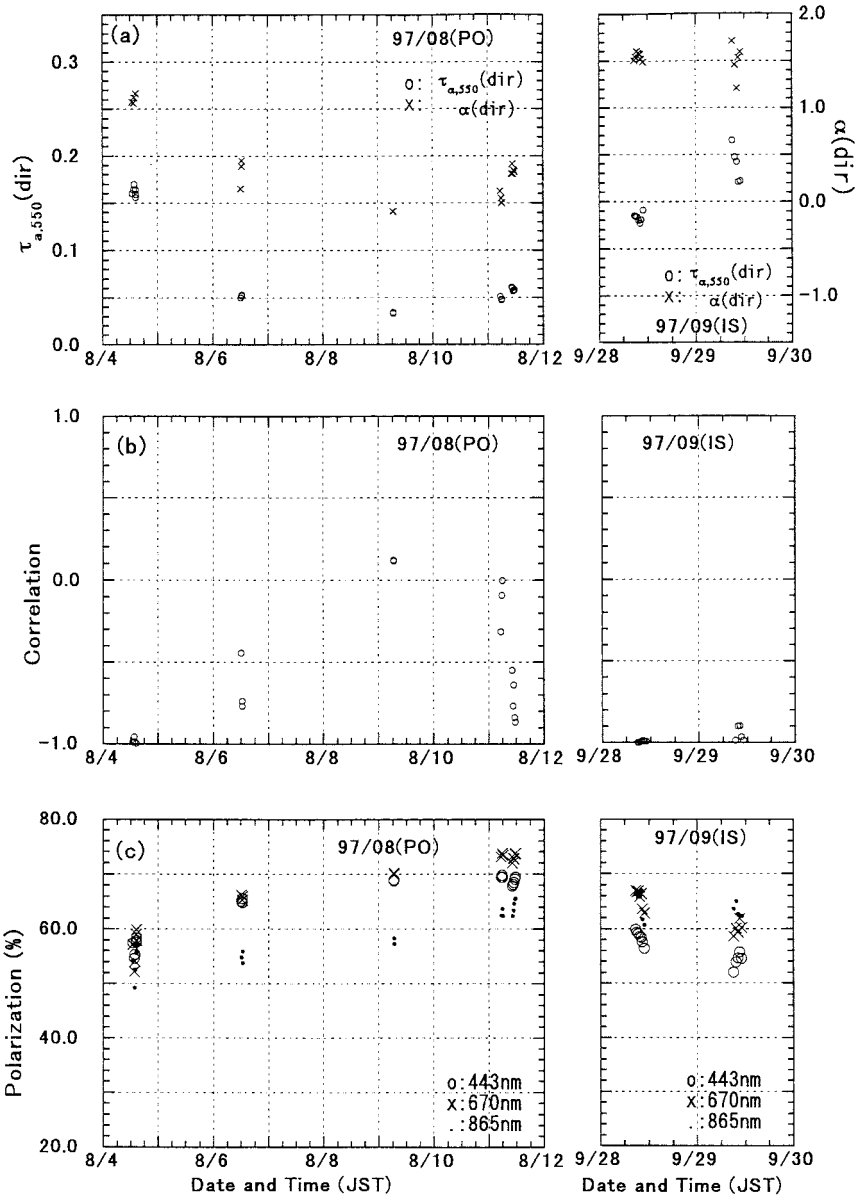

FIG. 2. (a) Aerosol optical thickness at $\lambda = 550$ nm (circles) and the Ångström coefficient (crosses) determined from the measurements of the direct solar radiation; (b) correlation coefficient between $\ln\tau_{a,\lambda}$ and $\ln\lambda$; (c) degree of linear polarization (%) measured by a multichannel polaimeter at $\lambda = 443$ nm (circles), 670 nm (crosses), and 865 nm (dots). Date and time are given in the Japanese Standard Time.

to retrieve the aerosol optical thickness and Ångström coefficient simultaneously from p_{90} measurements at two wavelengths. Among these wavelength combinations, the (443 nm, 865 nm) pair seems to be most suitable for precisely retrieving the aerosol optical thickness and Ångström coefficient considering the spread of the p_{90} space and the orthogonality between $\tau_{a,550}$ and α isolines. Visualization and error analysis of multiple measurements are discussed in detail by Post (1996). In this study, we simply estimated the $\tau_{a,550}$ and α retrieval errors caused by the measurement errors of p_{90} by $\pm 2\%$ in polarization units. In Table 4, absolute errors of $\tau_{a,550}$ and α are shown for $\tau_{a,550} = 0.04$, 0.16, and 0.64 and $\alpha = 0.24$ and 1.42. The larger value is shown when resultant errors differ from each other for opposite signs of measurement errors. Note that the errors discussed here are those caused by measurement errors on the assumption that the aerosol model is exact. For the measurement errors considered here, retrieval errors of $\tau_{a,550}$ are less than 0.01, 0.02, and 0.08 for $\tau_{a,550} = 0.04$, 0.16,

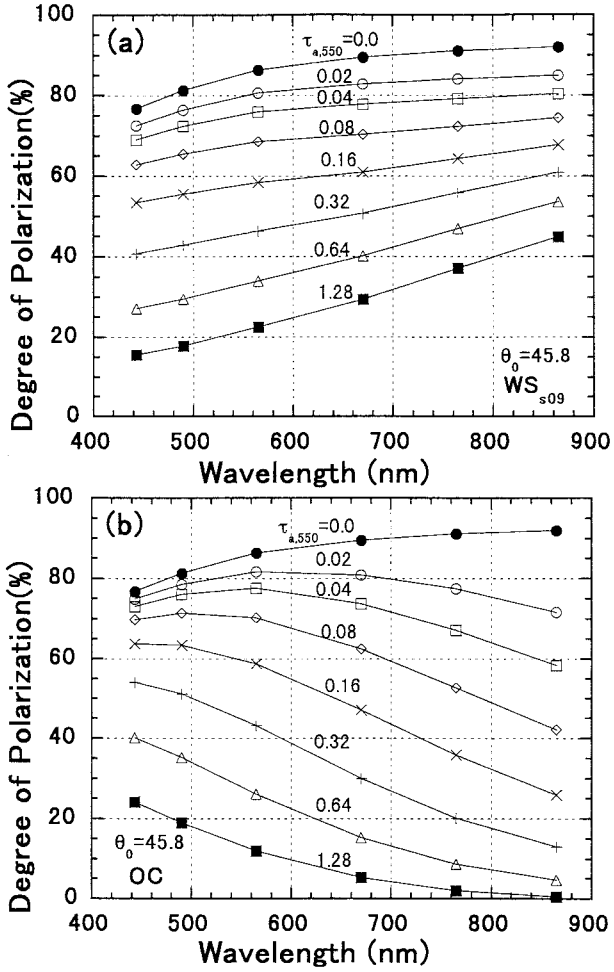

FIG. 3. Degree of linear polarization as a function of wavelength for (a) the water soluble model (WS_{s09}) and (b) the oceanic model (OC) at the solar zenith angle (θ_0) of 45.8° obtained from radiative transfer calculations. Here $\tau_{a,550}$ denotes the aerosol optical thickness at $\lambda = 550$ nm.

and 0.64, respectively. Retrieval errors of α are less than 0.1 for $\tau_{a,550} = 0.16$, and 0.64 whereas it is larger than 0.3 when $\tau_{a,550}$ is as small as 0.04.

b. Retrieval of aerosol optical thickness and Ångström coefficient from the degree of polarization

The aerosol optical thickness and the Ångström coefficient were retrieved from the measurements of p_{90} at $\lambda = 443$ and 865 nm by referring to the lookup table. First, the p_{90} values from the radiative transfer calculations for eight $\tau_{a,550}$ and six f_w values described in section 2 were interpolated with respect to the cosine of the solar zenith angle at the time of measurement. Next, these p_{90} values were refined by interpolating them with respect to $\tau_{a,550}$ and f_w for $\tau_{a,550} = 0.0$ to 1.28 (step = 0.0025), and $f_w = 0.0$ to 1.0 (step = 0.01). Third, a two-dimensional table of p_{90} was created as functions of $\tau_{a,550}$ and α using the relationship between f_w and α. Finally, we selected the ($\tau_{a,550}$, α) pair, which minimizes the following equation as the most probable values:

$$\sum_{i=1}^{2} [p_{90,\mathrm{cal}}(\lambda_i, \tau_{a,550}, \alpha) - p_{90,\mathrm{meas}}(\lambda_i)]^2, \qquad (7)$$

where λ_i refers to the wavelengths used in retrieval. Figures 5a and 5b show, respectively, the comparison of the aerosol optical thickness at $\lambda = 550$ nm and the Ångström coefficient retrieved from p_{90} at $\lambda = 443$ and 865 nm [$\tau_{a,550}(p_{90})$ and $\alpha(p_{90})$] with those determined from the direct solar radiation [$\tau_{a,550}$(dir) and α(dir)]. As a measure of the reliability of retrieval, the root-mean-square differences of p_{90} values between the calculations and measurements were computed by

$$\mathrm{rms}_{90} = \left\{ \frac{1}{6} \sum_{i=1}^{6} [p_{90,\mathrm{cal}}(\lambda_i, \tau_{a,550}, \alpha) - p_{90,\mathrm{meas}}(\lambda_i)]^2 \right\}^{1/2}. \qquad (8)$$

Rms_{90} values were less than 2% for all measurements.

Table 5 (line 1) shows the mean and standard deviation of the difference between $\tau_{a,550}(p_{90})$ and $\tau_{a,550}$(dir) and between $\alpha(p_{90})$ and α(dir). The aerosol optical thicknesses agree well with each other. However, the Ångström coefficient retrieved from p_{90} is larger than that from the direct solar radiation by 0.23. The difference is mainly caused by the fact that $\alpha(p_{90})$ is larger than α(dir) by about 0.5 when α(dir) is less than 0.5 (Fig. 5b), for which the optical thickness is less than 0.05 (Fig. 2a). This large difference between $\alpha(p_{90})$ and α(dir) is partly because the α(dir) determined from the direct solar radiation measurements is not very reliable and partly because the accuracy of $\alpha(p_{90})$ is much influenced by the measurement error of p_{90} for small aerosol optical thickness as mentioned in section 3.

Other wavelength pairs [(443 nm, 670 nm) and (670 nm, 865 nm)] were also examined. The results were similar to those in Fig. 4. The mean and standard deviation of the differences between $\tau_{a,550}(p_{90})$ and $\tau_{a,550}$(dir) and between $\alpha(p_{90})$ and α(dir) are shown in Table 5 (lines 2 and 3). The results of aerosol optical thickness retrieval are similar to that using 443- and 865-nm wavelength data. The results of Ångström coefficient retrieval differs from that using 443- and 865-nm wavelength data by about 0.1. The rms_{90} values were generally a little bit larger, reaching 3% in some cases.

A similar method was applied using all six channels (Table 5, lines 4). The only difference in Eq. (7) is that the summation is performed over six channels. As expected, the rms_{90} was improved compared to the two-channel method. It was generally less than 1%. However, the mean and standard deviation of the differences between $\tau_{a,550}(p_{90})$ and $\tau_{a,550}$(dir) and between $\alpha(p_{90})$ and α(dir) are similar to those by the two-channel method using 443 and 865nm. This is because two unknown parameters, $\tau_{a,550}$ and α, are considered in this algorithm, where two channels are essential and the other four channels provide only a slight improvement.

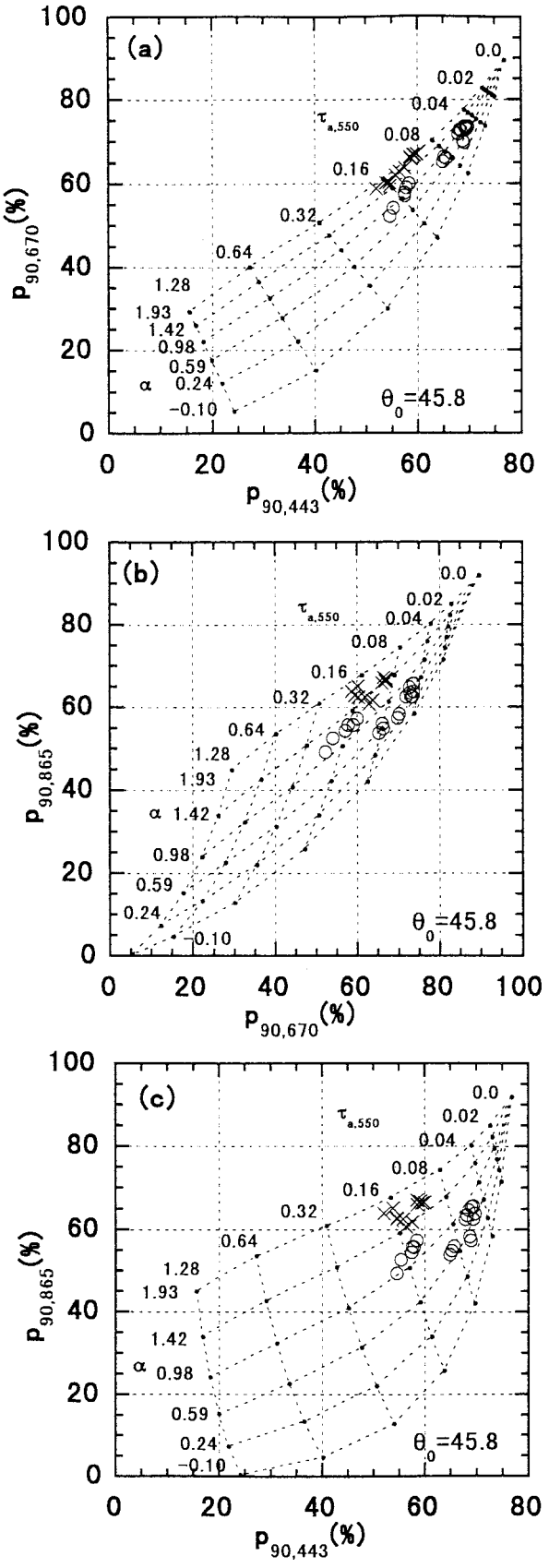

5. Discussion

The aerosol optical thickness and Ångström coefficient retrieved from the polarization measurements in section 4 are the effective values in the sense that the observed polarization values are reproduced by the radiative transfer calculations for a given aerosol size distribution model and the refractive indices based on Radiation Commission reports (WCP-55 1983; WCP-112 1986) with a modification of size distribution parameter.

The size distribution parameters and the refractive indices may be altered by, for example, the change of the ambient atmospheric relative humidity. Shettle and Fenn (1979) compiled the influence of relative humidity on the median radius of the lognormal size distribution parameters and the refractive index for aerosol of the lower atmosphere based on a number of previous studies. In this paper, the effect of the change of relative humidity on the retrieval algorithm is not explicitly examined. Instead of this, sensitivity tests are done separately to estimate the effect of the size distribution parameters and the refractive index on the retrieval algorithm. The aerosol model is again assumed to be the externally mixed model of the oceanic and water soluble components.

The size distribution parameters (r_m and σ) are changed for the oceanic or water soluble component, with the other component being the same as the reference model (OC or WS_{s09}). The refractive indices of the aerosol are fixed as before. From Table 2, four oceanic models (OC_{s08}, OC_{s12}, OC_{r05}, and OC_{r15}) and two water soluble models (WS_{s08} and WS_{r05}) are chosen for comparisons. The Ångström coefficient by these mixed aerosol models basically covers the range determined from the direct solar radiation measurements. For example, it ranges from -0.10 to 1.96 for the aerosol model composed of OC and WS_{r05} components. Other water soluble models are not suitable for further discussion because of their small α values.

First, we prepared synthesized measurement data of p_{90} at $\lambda = 443$ and 865 nm for $\tau_{a,550} = 0.04$, 0.16, and 0.64 and $\alpha = 0.24$ and 1.42 by the radiative transfer calculations based on the reference aerosol model (OC–WS_{s09}). Then, $\tau_{a,550}$ and α were retrieved using the above modified aerosol models. Differences from the true values are shown in Table 6 (lines 1–6), which correspond to the influence of the size distribution parameters on the retrieval. The $\tau_{a,550}$ values are not influenced very much by the above changes of size distribution param-

←

FIG. 4. Relationship of the degree of polarization between two wavelengths as a function of the aerosol optical thickness at $\lambda = 550$ nm ($\tau_{a,550}$) and the Ångström coefficient (α) for the solar zenith angle (θ_0) of 45.8°; (a) 443 nm vs 670 nm, (b) 670 nm vs 865 nm, and (c) 443 nm vs 865 nm. Dotted lines denote the calculations, whereas circles (crosses) denote measurements in the Pacific Ocean cruise (the Inland Sea of Japan cruise).

TABLE 4. Absolute errors of retrieval of the aerosol optical thickness at $\lambda = 550$ nm ($|\Delta\tau_{a,550}|$) and the Ångström coefficient ($|\Delta\alpha|$) caused by the measurement error of p_{90} by $\pm 2\%$ at $\lambda = 443$ and 865 nm. Solar zenith angle is 45.8°.

Wavelength (mm)	$\tau_{a,550}$	$\lvert\Delta\tau_{a,550}\rvert$						$\lvert\Delta\alpha\rvert$					
		0.04		0.16		0.64		0.04		0.16		0.64	
	α	0.24	1.42	0.24	1.42	0.24	1.42	0.24	1.42	0.24	1.42	0.24	1.42
443		0.01	0.01	0.02	0.02	0.06	0.08	0.33	0.33	0.10	0.07	0.02	0.05
865		0.00	0.00	0.01	0.01	0.02	0.02	0.07	0.14	0.05	0.09	0.07	0.07

eters of the oceanic component. However, $\tau_{a,550}$ is overestimated by larger than 30% for the OC–WS_{s08} model for $\tau_{a,550} = 0.64$ and $\alpha = 1.42$. This large difference is partly because the characteristic of the aerosol appears clearly when the aerosol optical thickness is much larger than the molecule optical thickness and partly because the water soluble component is optically dominant at $\alpha = 1.42$ ($f_w = 0.8$). The above changes of size distribution parameters affect the Ångström coefficient by less than 0.06.

Next, we retrieved the $\tau_{a,550}(p_{90})$ and $\alpha(p_{90})$ using the ship measurement data for the above modified aerosol models by the two-channel method (443 nm and 865 nm). Table 7 (lines 1–6) is the same as Table 5 (line 1) except that the modified aerosol models are used for retrieval. Figure 6 is the same as Fig. 5 except that the aerosol models are OC–WS_{r05} and OC_{s09}–WS_{s12}. By comparison of these results, we conclude that the retrieved $\tau_{a,550}(p_{90})$ and $\alpha(p_{90})$ are not significantly influenced by the changes of size distribution parameters considered here. This is partly because the aerosol optical thickness is small (<0.2) in our measurements.

Similarly, we examined the effects of the refractive indices of aerosol on the retrieval of $\tau_{a,550}$ and α. The aerosol size distribution is fixed to the reference model (OC–WS_{s09}). The real part of the oceanic component is changed by $+0.2$, $+0.1$, $+0.05$, and -0.05 from the original values (Table 1); for the water soluble component, $+0.05$, -0.05, -0.1, -0.2. The real part ranges from 1.32 to 1.58 for both components by these changes. The imaginary part is assumed to be 0.0, -0.005, -0.01, and -0.03, independent of the wavelength. The ranges of the Ångström coefficient were $-0.12 \sim -0.08$ for the oceanic component and $1.83 \sim 2.05$ for the water soluble component. Using synthesized measurement data, influence of the aerosol refractive index on the retrieval of $\tau_{a,550}$ and α is estimated (Table 7, lines 7–22). For the change of the real part by ± 0.05, relative difference of $\tau_{a,550}$ is less than 30%, absolute difference is less than 0.13, and difference of α is less than 0.12. The change of the real part by >0.1 may cause the relative difference larger than 30% for $\tau_{a,550}$ retrieval and the difference larger than 0.2 for α retrieval.

The imaginary part of the oceanic model is almost 0 whereas that of the water soluble model ranges from -0.005 to -0.012, depending on the wavelength (Table 1). Influences on the $\tau_{a,550}$ and α retrieval generally become larger as the imaginary value deviates from the original one. Especially, the optical thickness is overestimated with increasing the absolute of the imaginary part of the oceanic component. This is mainly because only scattered components are basically included in the sky radiation at a 90° angle from solar direction while both scattering and absorbing components are included in the optical thickness. The effect of changes of the imaginary part of the water soluble component is not

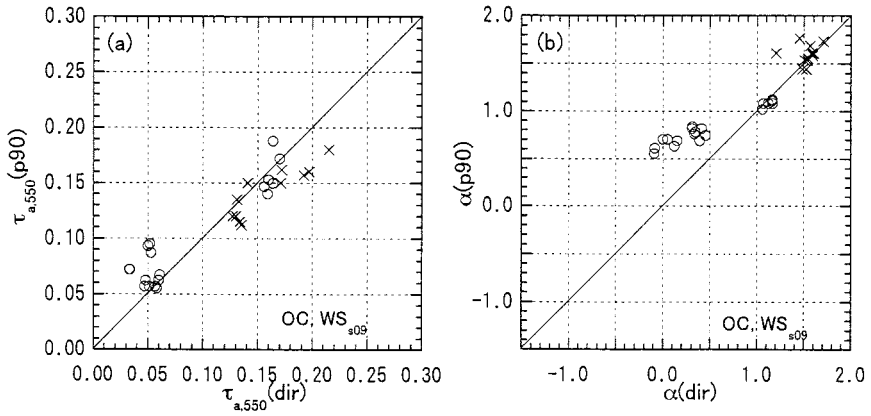

FIG. 5. (a) Comparison of the aerosol optical thickness at $\lambda = 550$ nm retrieved from the measurements of the degree of polarization at $\lambda = 443$ and 865 nm [$\tau_{a,550}(p_{90})$] with those determined from the direct solar radiation [$\tau_{a,550}$(dir)]. (b) Same as (a) but for the Ångström coefficient [$\alpha(p_{90})$ and α(dir)]. Circles (crosses) denote the PO (IS) cruise. Aerosol model is the reference model (OC and WS_{s09}).

TABLE 5. Mean and standard deviation (std dev) of the difference between the aerosol optical thickness at $\lambda = 550$ nm and the Ångström coefficient retrieved from polarization measurements [$\tau_{a,550}(p_{90})$ and $\alpha(p_{90})$] and those determined from the direct solar radiation measurements [$\tau_{a,550}$(dir) and α(dir)].

Aerosol models			$\tau_{a,550}(p_{90}) - \tau_{a,550}$(dir)		$\alpha(p_{90}) - \alpha$(dir)	
Oceanic	Water soluble	Wavelengths	Mean	Std dev	Mean	Std dev
OC	WS_{s09}	443, 865	0.00	0.02	0.23	0.27
OC	WS_{s09}	443, 670	0.00	0.02	0.37	0.34
OC	WS_{s09}	670, 865	−0.01	0.02	0.13	0.22
OC	WS_{s09}	6 wavelengths	0.00	0.02	0.23	0.24

large on the retrieval of α. However, errors larger than 0.2 are seen when that of the oceanic component is −0.03.

Table 7 (lines 7–22) is the same as Table 5 (line 1) except that the modified aerosol models are used for retrieval. By comparing these results with Table 5 (line 1), it is found that the effect of changes of the real part by ±0.05 is not large for on the retrieval of the optical thickness and Ångström coefficient for the measurements discussed in this study. As for the imaginary part, the accuracy of retrieving $\tau_{a,550}$ and α is not influenced very much except for $n_i = -0.03$ for the water soluble component and $n_i = -0.01$ and -0.03 for the oceanic component.

Up to this point, the real and imaginary parts are assumed to change independently. It is more realistic to change these parameters simultaneously. According to Shettle and Fenn (1979), both the real part and the absolute of the imaginary part increase with decreasing the relative humidity. As shown in Table 6, the difference in retrieval of the optical thickness has opposite sign with increasing the real part and the absolute of the imaginary part. The consistency of the $\tau_{a,550}$ retrieved from polarization measurements with those determined from the direct solar radiation discussed in section 4 suggests that the assumed refractive indices are basically not far from the real ones. Also, the effect of the alternations of the real and imaginary parts caused by the change of the relative humidity might be canceled out.

Another problem is the particle shapes. Previous theoretical studies (Asano 1980; Mishchenko and Travis 1994) show that the degree of polarization by nonspherical particles is different from that by spheres. Our assumption of sphericity of the maritime aerosol particles might cause an additional uncertainty in the retrieval. Further studies are needed to estimate the effect of the particle shapes on the inversion algorithm.

The inversion algorithm presented in this paper might be basically applicable to the retrieval of the effective optical thickness and Ångström coefficient of aerosols over the ocean from satellite polarization measurements. It should be noted, however, that the direction of a 90° angle from the solar direction is often near the sun glint region for satellite measurements, where information from the atmosphere is significantly contaminated by the radiation reflected from the ocean surface (Masuda 1998). Determining the feasibility of applying our method to the satellite data requires more sensitivity studies considering the solar and satellite geometry.

6. Conclusions

Sky radiation was measured with a portable multichannel polarimeter on the Pacific Ocean and on the Inland Sea of Japan in 1997 to investigate the feasibility of retrieving aerosol optical properties from polarization measurements. The degree of polarization was measured at a 90° angle from the solar direction in the principal plane. The direct solar radiation was also measured simultaneously. Both measurements were made at wavelengths of 443, 490, 565, 670, 765, and 865 nm. We carried out the radiative transfer calculations using the doubling–adding method to create a lookup table. The aerosol model over the ocean is assumed to be composed of the oceanic and the water soluble components of which size distributions are expressed by the lognormal function. Size distribution parameters and the refractive indices of aerosols are adopted from International Radiation Commission reports (WCP-55 1983; WCP-112 1986) with a modification.

The effective aerosol optical thickness and the Ångström coefficient were retrieved from measurements of the degree of polarization at wavelengths of 443 and 865 nm by referring to the lookup table. The retrieved values were compared with those determined from the direct solar radiation measurements. The mean and standard deviation of the difference of aerosol optical thickness retrieved from polarization measurements and those determined from the direct solar radiation were 0.00 and 0.02. The retrieved Ångström coefficients agreed well with those derived from the direct solar radiation measurements when the optical thickness exceeded 0.1, whereas the difference was about 0.5 when the aerosol optical thickness was as small as 0.05. This discrepancy may be partly because the accuracy of the Ångström coefficient determined from the direct solar radiation is poor and partly because the accuracy of retrieval of the Ångström coefficient is greatly influenced by the measurement error of the degree of polarization for small aerosol optical thickness. The retrieval using six wavelength measurement data shows little improvements compared to the two-wavelength

TABLE 6. Influence of the size distribution parameters (lines 1–6), the real part of the refractive index (lines 7–14), and the imaginary part of the refractive index (lines 15–22) of the aerosol models on the retrieval of the aerosol optical thickness ($\Delta\tau_{a,550}$) and the Ångström coefficient ($\Delta\alpha$) evaluated by numerical simulations. Retrieval errors using different aerosol models are shown for the synthesized measurement data calculated for the reference aerosol model (OC, WS_{s09}). Subscripts snn and rnn are the same as Table 2. Superscript $n_r + n{\cdot}nn$ ($n_r - n{\cdot}nn$) denotes that the real part of the refractive index (Table 1) is increased (decreased) by $n{\cdot}nn$. Superscript $n_i = n{\cdot}nn$ denotes that the imaginary part of the refractive index (Table 1) is replaced by $n{\cdot}nn$. Solar zenith angle is 45.8°.

			$\Delta\tau_{a,550}$						$\Delta\alpha$					
		$\tau_{a,550}$	0.04		0.16		0.64		0.04		0.16		0.64	
	Aerosol models	α	0.24	1.42	0.24	1.42	0.24	1.42	0.24	1.42	0.24	1.42	0.24	1.42
1	OC	WS_{s08}	0.00	0.01	0.01	0.03	0.07	0.22	0.03	0.00	0.05	0.00	0.03	−0.03
2	OC	WS_{r05}	0.00	0.00	0.00	0.01	0.01	0.05	0.02	0.00	0.02	0.02	0.01	0.02
3	OC_{s08}	WS_{s09}	0.00	0.00	−0.01	0.00	−0.06	−0.01	−0.06	0.02	−0.04	0.02	−0.03	0.02
4	OC_{s12}	WS_{s09}	0.01	0.00	0.02	0.00	0.08	0.02	0.03	−0.04	−0.01	−0.04	−0.04	−0.04
5	OC_{r05}	WS_{s09}	0.00	0.00	−0.01	0.00	−0.04	−0.01	0.02	0.01	−0.02	0.01	0.00	0.01
6	OC_{r15}	WS_{s09}	0.00	0.00	0.01	0.00	0.05	0.01	0.04	−0.03	0.01	−0.01	−0.01	−0.01
7	OC	$WS_{s09}^{nr+0.05}$	0.00	−0.01	−0.01	−0.02	−0.03	−0.09	−0.04	0.04	−0.01	0.06	−0.01	0.06
8	OC	$WS_{s09}^{nr-0.05}$	0.00	0.01	0.01	0.02	0.03	0.11	0.01	0.01	0.02	−0.02	0.01	−0.04
9	OC	$WS_{s09}^{nr-0.10}$	0.00	0.01	0.01	0.05	0.07	0.24	0.07	0.01	0.05	−0.04	0.01	−0.06
10	OC	$WS_{s09}^{nr-0.20}$	0.01	0.03	0.03	0.12	0.14	0.52	0.17	0.02	0.11	−0.06	0.02	−0.06
11	$OC^{nr+0.20}$	WS_{s09}	−0.01	0.00	−0.05	−0.01	−0.18	−0.04	0.32	0.21	0.32	0.19	0.32	0.19
12	$OC^{nr+0.10}$	WS_{s09}	−0.01	0.00	−0.03	−0.01	−0.11	−0.03	0.22	0.11	0.16	0.11	0.16	0.11
13	$OC^{nr+0.05}$	WS_{s09}	−0.01	0.00	−0.02	−0.01	−0.06	−0.02	0.10	0.09	0.10	0.07	0.08	0.07
14	$OC^{nr-0.05}$	WS_{s09}	0.01	0.00	0.03	0.01	0.13	0.03	−0.05	−0.06	−0.07	−0.09	−0.12	−0.09
15	OC	$WS_{s09}^{ni=0.0}$	0.00	0.00	−0.01	−0.01	−0.02	−0.06	0.05	0.08	0.01	0.08	0.01	0.11
16	OC	$WS_{s09}^{ni=-0.005}$	0.00	0.00	0.00	0.00	0.00	−0.01	0.04	0.11	0.01	0.08	0.01	0.08
17	OC	$WS_{s09}^{ni=-0.01}$	0.00	0.00	0.00	0.01	0.01	0.05	0.04	0.08	0.02	0.06	0.02	0.06
18	OC	$WS_{s09}^{ni=-0.03}$	0.00	0.01	0.01	0.05	0.07	0.33	0.09	0.05	0.05	0.00	0.02	−0.02
19	$OC^{ni=0:0}$	WS_{s09}	0.00	0.00	0.00	0.00	0.00	0.00	0.03	0.02	0.00	0.00	0.00	0.00
20	$OC^{ni=-0.005}$	WS_{s09}	0.01	0.00	0.04	0.01	0.30	0.06	0.04	−0.02	0.04	−0.05	−0.07	−0.07
21	$OC^{ni=-0.01}$	WS_{s09}	0.02	0.00	0.08	0.02	0.54	0.12	0.04	−0.11	0.02	−0.09	−0.08	−0.14
22	$OC^{ni=-0.03}$	WS_{s09}	0.05	0.01	0.25	0.05	0.64	0.39	0.05	−0.22	−0.04	−0.26	−0.04	−0.39

TABLE 7. Same as Table 5 but for different aerosol models. Subscripts snn and rnn are the same as Table 2. Superscripts $n_r + n{\cdot}nn$, $n_r - n{\cdot}nn$, and $n_i = n{\cdot}nn$ are the same as Table 6.

	Aerosol models		$\tau_{a,550}(p_{90}) - \tau_{a,550}(\text{dir})$		$\alpha(p_{90}) - \alpha(\text{dir})$	
	Oceanic	Water soluble	Mean	Std dev	Mean	Std dev
1	OC	WS_{s08}	0.02	0.02	0.23	0.31
2	OC	WS_{r05}	0.00	0.02	0.26	0.27
3	OC_{s08}	WS_{s09}	0.00	0.02	0.23	0.26
4	OC_{s12}	WS_{s09}	0.00	0.02	0.20	0.27
5	OC_{r05}	WS_{s09}	0.00	0.02	0.24	0.27
6	OC_{r15}	WS_{s09}	0.00	0.02	0.22	0.27
7	OC	$WS_{s09}^{nr+0.05}$	−0.01	0.03	0.27	0.24
8	OC	$WS_{s09}^{nr-0.05}$	0.01	0.02	0.22	0.30
9	OC	$WS_{s09}^{nr-0.10}$	0.03	0.02	0.23	0.32
10	OC	$WS_{s09}^{nr-0.20}$	0.08	0.03	0.26	0.37
11	$OC^{nr+0.20}$	WS_{s09}	−0.01	0.02	0.50	0.34
12	$OC^{nr+0.10}$	WS_{s09}	−0.01	0.02	0.39	0.31
13	$OC^{nr+0.05}$	WS_{s09}	0.00	0.02	0.32	0.29
14	$OC^{nr-0.05}$	WS_{s09}	0.01	0.02	0.13	0.26
15	OC	$WS_{s09}^{ni=0.0}$	−0.01	0.02	0.30	0.25
16	OC	$WS_{s09}^{ni=-0.005}$	0.00	0.02	0.29	0.26
17	OC	$WS_{s09}^{ni=-0.01}$	0.00	0.02	0.29	0.27
18	OC	$WS_{s09}^{ni=-0.03}$	0.03	0.02	0.27	0.30
19	$OC^{ni=0.0}$	WS_{s09}	0.00	0.02	0.24	0.27
20	$OC^{ni=-0.005}$	WS_{s09}	0.01	0.03	0.20	0.28
21	$OC^{ni=-0.01}$	WS_{s09}	0.02	0.03	0.16	0.29
22	$OC^{ni=-0.03}$	WS_{s09}	0.05	0.04	0.00	0.31

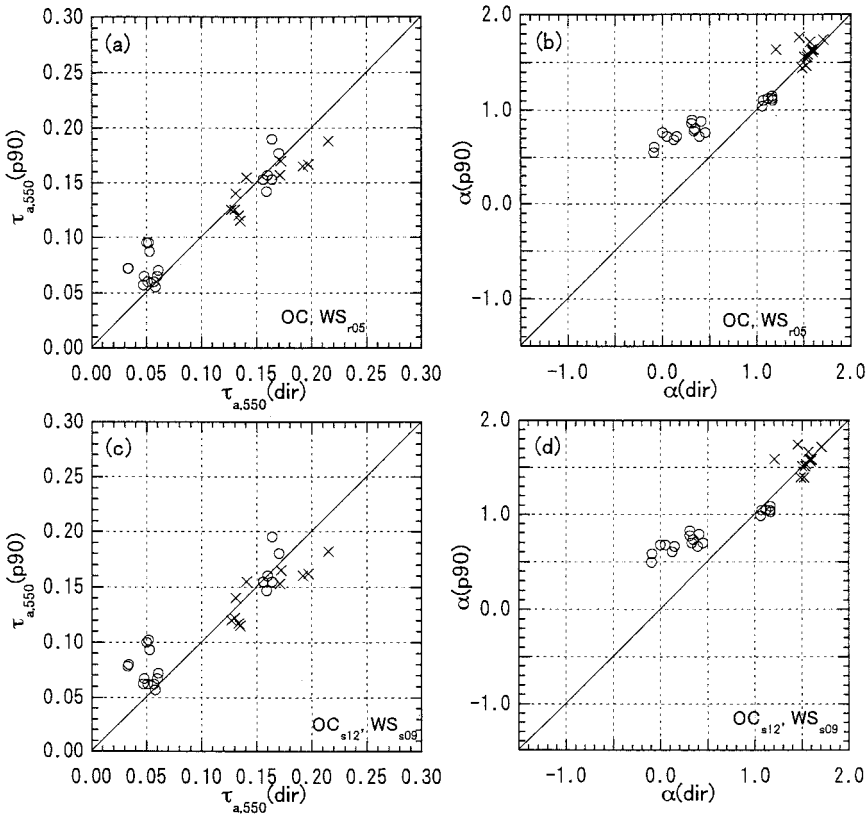

FIG. 6. The same as Fig. 5 but for different aerosol models (a), (b) OC and WS_{r05}; (c), (d) OS_{s12} and WS_{s09}.

method because two unknowns are considered in the inversion algorithm.

We examined the possible errors in the model assumptions using synthesized measurement data for the aerosol optical thickness of 0.04, 0.16, and 0.64. The retrieval of aerosol optical thickness were not influenced very much by the changes of the median radius by 50% and σ value by 20% for the oceanic component. However, relative errors larger than 30% appeared for the change of σ value by 10% for the water soluble component when the aerosol optical thickness was as large as 0.64. For the change of the real part of the refractive index of the oceanic or the water soluble aerosol component by ± 0.05, the relative error of the optical thickness was less than 30%, the absolute error was less than 0.13, and the error in the Ångström coefficient retrieval was less than 0.12. The original values of the imaginary part were almost 0 for the oceanic model and -0.005 to -0.012 for the water soluble model depending on the wavelength. Overestimation of the retrieved aerosol optical thickness was clearly seen with increasing the absolute value of the imaginary part as large as -0.01 for the oceanic component and -0.03 for the water soluble component. The retrieval of the Ångström coefficient was not much influenced by the changes of the imaginary part of the refractive index of the water soluble component ranging from 0.0 to -0.03. However, retrieval error of the Ångström coefficient by larger than 0.2 was shown when the imaginary part of the refractive index of -0.03 was used for the oceanic component.

From an observational point of view, it should be emphasized that measuring the degree of polarization is easier than measuring the intensity or transmittance of radiation because it is a relative value in that critical calibration is not required. Further, the degree of polarization at a 90° angle from the solar direction generally shows the maximum value with respect to the observation direction, which enables us to make stable measurements of polarization despite ship motions.

Acknowledgments. We are grateful to the members of the Institute for Sea-Training, Ministry of Transport of Japan, and the captains and crews of the training ships *Seiun-maru* and *Fukae-maru* for their cooperation with the observations. We sincerely thank Drs. S. Mukai and I. Sano of Kinki University for their helpful discussions on interpreting measurements from the ship. We thank anonymous reviewers for their insightful comments. Part of this study was supported by the Ministry of Education, Culture, and Sport of Japan, and the National Space Development Agency of Japan.

REFERENCES

Ahern, F. J., R. P. Gauthier, P. M. Teillet, J. Sirois, G. Fedosejevs, and D. Lorente, 1991: Investigation of continental aerosols with high-spectral-resolution solar-extinction measurements. *Appl. Opt.*, **30,** 5276–5287.

Ångström, A., 1964: The parameters of atmospheric turbidity. *Tellus,* **16,** 64–75.

Asano, S., and M. Sato, 1980: Light scattering by randomly oriented spheroidal particles. *Appl. Opt.,* **19,** 962–974.

Coulson, K. L., 1980: Characteristics of skylight at the zenith during twilight as indicators of atmospheric turbidity. 1: Degree of polarization. *Appl. Opt.,* **19,** 3469–3480.

——, 1983: Effects of the El Chichon volcanic cloud in the stratosphere on the polarization of light from the sky. *Appl. Opt.,* **22,** 1036–1050.

Cox, C., and W. Munk, 1954: Statistics of the sea surface derived from sun glitter. *J. Mar. Res.,* **13,** 198–227.

d'Almeida, G. A., P. Koepke, and E. P. Shettle, 1991: *Atmospheric Aerosols.* A. Deepak, 561 pp.

DeLuisi, J. J., and Coauthors, 1976a: Results of a comprehensive atmospheric aerosol-radiation experiment in the southwestern United States. Part I: Size distribution, extinction optical depth and vertical profiles of aerosols suspended in the atmosphere. *J. Appl. Meteor.,* **15,** 441–454.

——, and Coauthors, 1976b: Results of a comprehensive atmospheric aerosol-radiation experiment in the southwestern United States. Part II: Radiation flux measurements and theoretical interpretation. *J. Appl. Meteor.,* **15,** 455–463.

Deschamps, P. Y., F. M. Bréon, M. Leroy, A. Podaire, A. Bricaud, J. C. Buriez, and G. Séze, 1994: The POLDER mission: Instrument characteristics and scientific objectives. *IEEE Trans. Geosci. Remote Sens.,* **32,** 598–615.

Deuzé, J. L., C. Devaux, M. Herman, R. Santer, J. Y. Balois, L. Gonzalez, P. Lecomte, and C. Verwaerde, 1989: Photopolarimetric observations of aerosols and clouds from balloon. *Remote Sens. Environ.* **29,** 93–109.

Fraser, R. S., S. Mattoo, E.-N. Yeh, and C. R. McClain, 1997: Algorithm for atmospheric and glint corrections of satellite measurements of ocean pigment. *J. Geophys. Res.,* **102,** 17 107–17 118.

Gordon, H. R., 1997: Atmospheric correction of ocean color imagery in the Earth Observing System era. *J. Geophys. Res.,* **102,** 17 081–17 106.

Hansen, J. E., and L. D. Travis, 1974: Light scattering in planetary atmospheres. *Space Sci. Rev.,* **16,** 527–610.

Higurashi, A., and T. Nakajima, 1997: An analysis of radiative fields in a coupled atmosphere–ocean system. *IRS'96: Current Problems in Atmospheric Radiation,* W. L. Smith and K. Stamnes, Eds., A. Deepak, 553–556.

Hoppel, W. A., J. W. Fitzgerald, G. M. Frick, and R. E. Larson, 1990: Aerosol size distributions and optical properties found in the marine boundary layer over the Atlantic Ocean. *J. Geophys. Res.,* **95,** 3659–3686.

Kaufman, Y. J., A. Gitelson, A. Karnieli, E. Ganor, R. S. Fraser, T. Nakajima, S. Mattoo, and B. N. Holben, 1994: Size distribution and scattering phase function of aerosol particles retrieved from sky brightness measurements. *J. Geophys. Res.,* **99,** 10 341–10 356.

——, and Coauthors, 1997: Passive remote sensing of tropospheric aerosol and atmospheric correction for the aerosol effect. *J. Geophys. Res.,* **102,** 16 815–16 830.

Kawata, Y., and A. Yamazaki, 1998: Multiple scattering analysis of airborne POLDER image data over the sea. *IEEE Trans. Geosci. Remote Sens.,* **36,** 51–60.

Kneizys, F. X., J. H. Chetwynd Jr., R. W. Fenn, E. P. Shettle, L. W. Abreu, R. A. McClatchey, W. O. Gallery, and J. E. A. Salby, 1980: Atmospheric transmittance/radiance: Computer code LOWTRAN5. Air Force Geophysics Laboratory Rep. AFGL-TR-80-0067, Hanscom AFB, MA, 233 pp. [Available from Air Force Geophysics Laboratory (OPI), Hanscom AFB, Massachusetts 01731.]

——, E. P. Shettle, L. W. Abreu, J. H. Chetwynd, G. P. Anderson, W. O. Gallery, J. E. A. Salby, and S. A. Clough, 1988: Users guide to LOWTRAN7. Air Force Geophysics Laboratory Rep. AFGL-TR-88-0177, Hanscom AFB, MA, 146 pp. [Available

from Air Force Geophysics Laboratory (OPI), Hanscom AFB, Massachusetts 01731.]

Korotaev, G. K., S. M. Sakerin, A. M. Ignatov, L. L. Stowe, and E. P. McClain, 1993: Sun-photometer observation of aerosol optical thickness over the North Atlantic from a Soviet research vessel for validation of satellite measurements. *J. Atmos. Oceanic Technol.*, **10,** 725–735.

Leroy, M., and Coauthors, 1997: Retrieval of atmospheric properties and surface bidirectional reflectances over land from POLDER/ADEOS. *J. Geophys. Res.,* **102,** 17 023–17 037.

Masuda, K., 1998: Effects of the speed and direction of surface winds on the radiation in the atmosphere–ocean system. *Remote Sens. Environ.,* **64,** 53–63.

——, and T. Takashima, 1988: Dependence of the radiation just above and below the ocean surface on atmospheric and oceanic parameters. *Appl. Opt.,* **27,** 4891–4898.

——, and M. Sasaki, 1997: A multi-spectral polarimeter for measurements of direct solar and diffused sky radiation: Calibration and measurements. *Opt. Rev.,* **4,** 496–501.

Mishchenko, M. I., and L. D. Travis, 1994: Light scattering by polydispersions of randomly oriented spheroids with sizes comparable to wavelengths of observation. *Appl. Opt.,* **33,** 7206–7225.

——, and ——, 1997: Satellite retrieval of aerosol properties over the ocean using polarization as well as intensity of reflected sunlight. *J. Geophys. Res.,* **102,** 16 989–17 013.

Nakajima, T., T. Takamura, M. Yamano, M. Shiobara, T. Yamauchi, R. Goto, and K. Murai, 1986: Consistency of aerosol size distributions inferred from measurements of solar radiation and aerosols. *J. Meteor. Soc. Japan,* **64,** 765–776.

——, G. Tonna, R. Rao, P. Boi, Y. Kaufman, and B. Holben, 1996: Use of sky brightness measurements from ground for remote sensing of particulate polydispersions. *Appl. Opt.,* **35,** 2672–2686.

Post, M. J., 1996: A graphical technique for retrieving size distribution parameters from multiple measurements: Visualization and error analysis. *J. Atmos. Oceanic Technol.,* **13,** 863–873.

Rao, C. R. N., T. Takashima, and R. B. Toolin, 1973: Measurements and interpretation of the polarization of radiation emerging from the atmosphere at an altitude of 28 km over south-western New Mexico (USA). *Quart. J. Roy. Meteor. Soc.,* **99,** 294–302.

Roger, J. C., R. Santer, M. Herman, and J. L. Deuzé, 1994: Polarization of the solar light scattered by the earth–atmosphere system as observed from the U. S. shuttle. *Remote Sens. Environ.,* **48,** 275–290.

Shettle, E. P., and R. W. Fenn, 1979: Models for the aerosols of the lower atmosphere and the effects of humidity variations on their optical properties. Air Force Geophysics Laboratory Rep. AFGL-TR-79-0214, Hanscom AFB, MA, 94 pp. [Available from Air Force Geophysics Laboratory (OPI), Hanscom AFB, Massachusetts 01731.]

Shiobara, M., and S. Asano, 1994: Estimation of cirrus optical thickness from sun photometer measurements. *J. Appl. Meteor.,* **33,** 672–681.

Takayama, Y., K. Masuda, and T. Takashima, 1991: Polarimetric investigation of the atmospheric aerosols over the Pacific Ocean. *Int. J. Remote Sens.,* **12,** 969–983.

Tanaka, M., T. Takamura, and T. Nakajima, 1983: Refractive index and size distribution of aerosols as estimated from light scattering measurements. *J. Climate Appl. Meteor.,* **22,** 1253–1261.

Tanré, D., M. Herman, and Y. J. Kaufman, 1996: Information on aerosol size distribution contained in solar reflected spectral radiances. *J. Geophys. Res.,* **101,** 19 043–19 060.

——, Y. J. Kaufman, M. Herman, and S. Mattoo, 1997: Remote sensing of aerosol properties over oceans using the MODIS/EOS spectral radiances. *J. Geophys. Res.,* **102,** 16 971–16 988.

Villevalde, Y. V., A. V. Smirnov, N. T. O'Neill, S. P. Smyshlyaev, and V. V. Yakovlev, 1994: Measurement of aerosol optical depth in the Pacific Ocean and the North Atlantic. *J. Geophys. Res.,* **99,** 20 983–20 988.

WCP-55, 1983: Report of the expert meeting on aerosols and their climate effects. World Meteorological Organization, Geneva, 107 pp.

WCP-112, 1986: A preliminary cloudless standard atmosphere for radiation computation. WMO/TD24, World Meteorological Organization, Geneva, 53 pp.

WMO, 1990: Report of the experts meeting on space observations of tropospheric aerosols and complementary measurements. WCRP-48, WMO/TD 389, Geneva, 51 pp.

Zhang, T., and H. R. Gordon, 1997: Retrieval of elements of the columnar aerosol scattering phase matrix from polarized sky radiance over the ocean: Simulations. *Appl. Opt.,* **36,** 7948–7959.

Zhao, F., Z. Gong, H. Hu, M. Tanaka, and T. Hayasaka, 1997: Simultaneous determination of the aerosol complex index of refraction and size distribution from scattering measurements of polarized light. *Appl. Opt.,* **36,** 7992–8001.